THE JOURNAL OF PHYSICAL CHEMISTRY C

Article

pubs.acs.org/JPCC

Insights into the Effect of Pt Atomic Ensemble on HCOOH Oxidation over Pt-Decorated Au Bimetallic Catalyst To Maximize Pt Utilization

Tian Duan, Riguang Zhang,* Lixia Ling, and Baojun Wang*

Key Laboratory of Coal Science and Technology of Ministry of Education and Shanxi Province, Taiyuan University of Technology, Taiyuan 030024, Shanxi, People's Republic of China

ABSTRACT: Density functional theory calculations have been employed to probe into a comparative study of HCOOH oxidation on Pt(111) and three PtAu(111) surfaces with different Pt atomic ensembles-decorated Au(111) surfaces, denoted as Pt ML, Pt_6Au_3, and Pt_3Au_6, respectively. Our results show that HCOOH dehydrogenation is dominant on PtAu(111) surface; as compared to Pt(111) surface, PtAu(111) surfaces are efficient for HCOOH dehydrogenation to CO_2, and show an inhibiting effect to HCOOH dehydration to CO. The catalytic activity and selectivity of PtAu(111) surfaces toward HCOOH oxidation are obviously dependent on the Pt atomic ensemble of the reaction active center. The enhanced catalytic activity and selectivity of PtAu bimetallic catalysts toward HCOOH oxidation should be attributed to their suppression to the dehydration reactions of HCOOH, which is well confirmed by the reported experimental results that the high catalytic activity of PtAu catalyst is caused by the increased selectivity toward HCOOH dehydrogenation. It is found that Pt ML surface, consisting of 1.0 monolayer Pt on an Au substrate, is not only efficient in the utilization of Pt, but also highly active and selective toward the dehydrogenation of HCOOH oxidation, which can suppress the formation of poisonous species CO. In addition, the present results may be helpful for the search of prospective substitutes to Pt electrode for hydrogen production in the direct formic acid fuel cell.

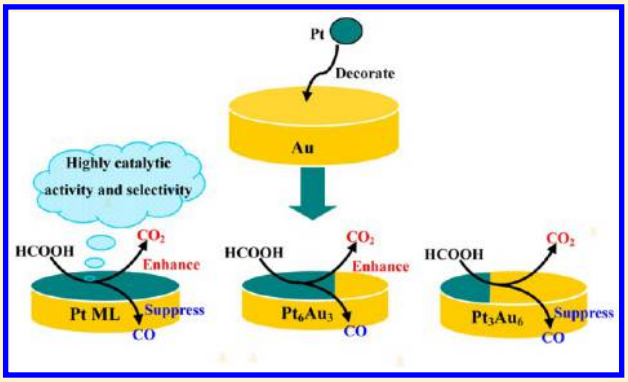

1. INTRODUCTION

Direct formic acid fuel cell (DFAFC) has been progressively recognized due to its advantages of high energy density, fast oxidation kinetics, and nontoxic nature of formic acid (HCOOH) as compared to methanol.[1−4] So DFAFC has been proposed as a possible replacement for the direct methanol fuel cell (DMFC).[5−8] It is generally known that both Pt-based and Pd-based catalysts are the most widely used two types of catalysts for HCOOH oxidation,[2,9−16] in which Pd-based catalyst possesses the high initial activity for this reaction because it is free of CO poisoning; however, the high catalytic performance cannot be sustained, as Pd dissolves in acidic solutions and is vulnerable toward the intermediate species.[12,15,17−19] Meanwhile, Pt, as the most widely used catalyst in DFAFC, is more resistant to corrosion, but the activity toward HCOOH oxidation is hindered by CO poisoning;[11,20,21] in addition, Pt is high cost, which also limits its widespread commercial applications.

For Pt-based catalyst, it is generally accepted that the electrochemical oxidation of HCOOH is thought to occur via a dual pathway mechanism consisting of direct and indirect pathways.[8,13,22−25] The direct pathway occurs via the dehydrogenation of HCOOH to form CO_2; this pathway cannot form CO, that is, $HCOOH \rightarrow CO_2 + 2H^+ + 2e^-$. In contrast, the indirect pathway proceeds by the dehydration of HCOOH to form CO, which may poison the electrode or be further oxidized to produce CO_2, $HCOOH \rightarrow CO + H_2O$; moreover, these pathways have been also proved over Pd catalyst.[26−28] Lee et al.[27] have suggested that the formic acid is oxidized to CO_2 through a dual pathway mechanism in Pd metal. Yoo et al.[28] have considered three different pathways of HCOOH decomposition via either the formate (HCOO) or the carboxyl (COOH) intermediates, in which the former pathway only produces CO_2, and the latter pathway produces both CO_2 and CO. To avoid CO poisoning toward the Pt-based catalysts, the direct pathway is highly desired, which can enhance the overall cell efficiency of DFAFC.[8,29]

Although the pure Pt catalyst is easily poisoned by CO, the modification of Pt with a second transition metal or noble metal to form binary Pt-based catalyst has been recognized as one of the most effective strategies to enhance the catalytic activity, selectivity, and durability toward HCOOH oxidation,[12,21,30] such as several PtM (M = Au, Pd, Fe, Pb, Ru, Sb, and Bi) bimetallic catalysts.[31−37] The surface reactivity of the modified Pt-based catalyst has been broadly explained by the "ensemble effect" (by changing the adsorption sites of the reactants)[38] and the "ligand effect" (by perturbing the electronic structure of the surface).[14,39−41]

Among various Pt-based bimetallic catalysts, due to good compatibility between Pt and Au, PtAu catalyst is one of the

Received: November 5, 2015
Revised: January 13, 2016
Published: January 19, 2016

DOI: 10.1021/acs.jpcc.5b10831
J. Phys. Chem. C 2016, 120, 2234−2246

most promising catalysts used for HCOOH oxidation,[42] and exhibits good catalytic activity and stability;[43] this is because Au can provide a synergistic catalytic effect that involves the suppression of adsorbed poisonous species and a change in electronic band structure to modify the adsorption strength of surface species.[44−46] Moreover, as compared to Pt, Au cannot be deactivated by CO poisoning under the realistic reaction conditions; however, Au exhibits a lower catalytic activity toward HCOOH oxidation,[22,47,48] and, as a result, previous studies by Adzic et al.[49] have modified Pt nanoparticles with Au clusters, suggesting that Au clusters can improve the stability by raising Pt oxidation potential. Yin and co-workers[12] have synthesized a novel Pt-around-Au nanocomposite by the electrostatic self-assembly, which significantly improves the catalytic activity toward HCOOH oxidation, and thus it is a promising catalyst in the application of DFAFC. Liu et al.[50] have prepared the carbon-supported PtAu alloy nanoparticle catalysts (PtAu/C), which presents the superior catalytic performance over the Pt/C catalyst by the electrocatalytic activity and durability measurements of HCOOH. Gojković and co-workers[51] have investigated HCOOH oxidation on Au-modified Pt and Pt-modified Au electrodes, and both types of PtAu surfaces are found to be more active toward HCOOH oxidation as compared to Pt catalyst. Chen et al.[14] have experimentally investigated the carbon-supported PtAu alloy nanoparticle catalysts (PtAu/C) for the enhanced electrocatalytic oxidation of HCOOH, suggesting that the high performance of PtAu/C catalyst can be attributed to the increased selectivity toward HCOOH dehydrogenation at the decreased availability of adjacent Pt atoms; moreover, the electrocatalytic activities of the catalysts strongly rely on the bimetallic PtAu composition. Huang et al.[52] have examined the effects of Au on the activity of HCOOH oxidation using the electrospun carbon nanofiber-supported PtAu bimetallic nanoparticles (PtAu/CNF), which presents improved catalytic activities as compard to Pt/CNF. Recently, Au has been studied as a catalyst for HCOOH oxidation using theoretical and experimental methods; the studies by Singh et al.[53] have shown that HCOOH oxidation follows the formate (HCOO)-mediated path, which can lead to 100% selectivity toward the dehydrogenation products (CO_2 + H_2) on Au(111), Au(100), and Au(211) surfaces.

Up to now, to the best of our knowledge, although the above experimental studies about HCOOH oxidation have shed light on the possible nature of active sites over PtAu catalyst, the understanding of the underlying mechanism for HCOOH oxidation over PtAu catalyst, as well as the effect of Pt contents on the catalytic activity of HCOOH oxidation, remain unelucidated theoretically at a molecular level; as a result, the comparison of catalytic activities becomes difficult, and hinders the establishment of the composition−activity relationships, which are critical for the rational design of highly efficient and active catalysts used in DFAFC. So far as we know, only Zhang et al.[54] have investigated the CO pathway and non-CO pathway of CH_3OH oxidation on Pt(111) and Pt_6Au_3(111) bimetallic surfaces using density functional theory (DFT) calculations, suggesting that the enhanced electrocatalytic activity of PtAu bimetallic catalyst for CH_3OH oxidation is due to the changing in major reaction pathway from the CO pathway on the pure Pt catalyst to the non-CO pathway, rather than the easier removal of CO on PtAu catalyst. In addition, the studies by Yuan and Liu[15] have indicated the particular importance of the ensemble effects to tune the activity and selectivity of PdAu bimetallic surface for HCOOH oxidation. Thus, to search for a novel catalyst with the improved catalytic activity of HCOOH oxidation and CO antipoisoning ability, and to provide a clue for rationally designing sustainable and cost-effective catalysts in DFAFC, it is necessary to probe into the structure-dependent oxidation of HCOOH over Pt-decorated Au bimetallic catalysts to maximum the utilization of Pt.

In this study, using DFT calculations, we have systematically investigated the detailed mechanism for the direct and indirect pathways of HCOOH oxidation on Pt(111) and three PtAu(111) surfaces with different Pt atomic ensembles incorporated into Au(111) surface. The results are expected to understand the mechanism of HCOOH oxidation over PtAu catalyst at the molecular level, and illustrate the effects of Pt modification with Au to substitute Pt catalyst and Pt contents on HCOOH oxidation, as well as elucidate the reason why PtAu bimetallic catalyst can enhance the catalytic activity and improve CO antipoisoning ability during HCOOH oxidation, which can serve as a foundational prototype to probe into the complex HCOOH oxidation on other catalyst systems.

2. COMPUTATIONAL DETAILS

2.1. Calculation Methods. All calculations have been performed in the framework of density functional theory (DFT) implemented by the Dmol^3 program package in Materials Studio 4.4;[55,56] the exchange-correlation effects are described with the generalized gradient approximation (GGA) using the PBE functional proposed by Perdew, Burke, and Ernzerhof.[57,58] The GGA-PBE functional has been widely used to investigate the oxidation of small molecules on noble metal surfaces, and the obtained results are often reliable.[9,24,59−62] A 3 × 3 × 1 Monkhorst−Pack k-point grid is used for the integrations of the Brillouin zone. The double-numerical basis set with a polarization d-function (DNP) is chosen to expand the valence electron functions.[63]

To determine accurate activation barriers of the reaction, the transition states (TSs) of the reactions are searched using the linear and quadratic synchronous transit (LST/QST) approach.[64] In addition, a vibrational frequency analysis has been calculated to validate the true nature of the saddle point by identifying only a single imaginary frequency along the reaction coordinate, and TS confirmation is performed on every transition state to confirm that they lead to the desired reactants and products.

The activation barrier (E_a) and reaction energy (ΔH) are calculated using the following equations:

$$E_a = E_{TS} - E_{IS}$$

$$\Delta H = E_{FS} - E_{IS}$$

where E_{IS}, E_{TS}, and E_{FS} are the total energies of the initial state (IS), transition state (TS), and final state (FS) for the reaction, respectively.

2.2. Surface Model. It is well-known that Pt(111) and Au(111) surfaces are the most stable crystal planes in the exposed basal planes of nanoparticles, so it is generally chosen as the representative surface for both experimental and theoretical studies.[54] Pt(111) and Au(111) surfaces are constructed by fcc lattice with the lattice constants of 3.924 and 4.078 Å for Pt and Au bulk, respectively, which are modeled by a four-layer periodic slab within a $p(3 \times 3)$ super cell with nine atoms at each layer. The vacuum gap is set to 15

DOI: 10.1021/acs.jpcc.5b10831
J. Phys. Chem. C 2016, 120, 2234−2246

Å in the z direction to separate the slabs, which is large enough to avoid the interactions between slabs.

On the other hand, to construct different Pt atomic distributions on bimetallic PtAu(111) surface, as shown in Figure 1, Au atoms on the outmost layer are replaced by Pt

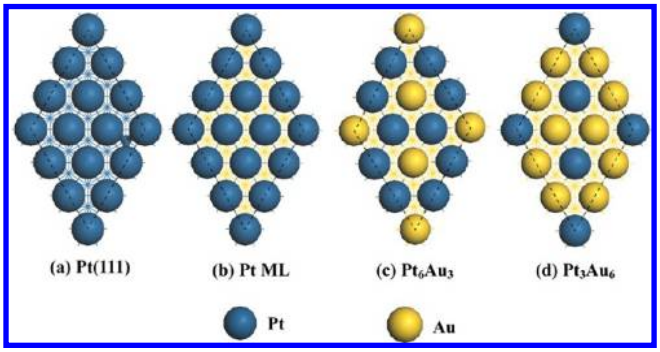

Figure 1. Unit cells and distribution of different Pt ensembles incorporated into Au(111) surface. The dotted lines are the boundaries of unit cells used in our calculations.

atoms; three PtAu(111) surfaces have been employed in this study, including the monolayer Pt substituted on Au(111) surface denoted as Pt ML surface, and Pt-decorated Au(111) surfaces named as Pt_6Au_3 and Pt_3Au_6 surfaces, respectively. Meanwhile, Pt_3Au_6, Pt_6Au_3, and Pt ML surfaces have been considered to represent the different Pt:Au surface ratios over the Au(111) surface; these three models are employed to approximately describe the formations of Pt monomer, Pt dimer, and Pt trimer over Au(111) surface when the surface Au atoms are replaced by three, six, and monolayer Pt atoms, respectively. During the calculations, the top two surface layers together with the adsorbed species are allowed to relax, while the bottom two surface layers are fixed at their bulk structure so to resemble the unperturbed bulk atoms. On Pt(111) and three PtAu(111) surfaces, four different adsorption sites exist: top, bridge, hcp, and fcc.

To clearly understand the stability of PtAu(111) surfaces with different Pt ensembles in surface layer, the formation energy of different Pt ensembles, E_f, has been considered, which is obtained by the following formulas:[65−67]

$$E_f = [E_{tot}(\text{decorated}) + nE_{Au} - E_{tot}(\text{pure}) - nE_{Pt}]/n$$

where E_{tot}(pure) and E_{tot}(decorated) are the total energies of pure Au(111) surface and the different Pt-decorated Au(111) surface; E_{Au} and E_{Pt} represent the total energies of single Au and Pt atoms calculated from the bulk metal materials, respectively; moreover, n corresponds to the number of Au atoms replaced by Pt atoms over Au(111) surface. With this definition, more positive values suggest that the formation of PtAu(111) surface is endothermic, which means the stability of PtAu(111) surface should be weaker than that of the pure Au(111) surface in the experiment. As a result, our calculated formation energies show that the stability order of PtAu(111) surfaces with different Pt ensembles is Pt_6Au_3 (0.30 eV) < Pt ML (0.40 eV) < Pt_3Au_6 (0.44 eV), indicating that these three Pt-decorated Au(111) surfaces are easily formed; moreover, the formation of Pt_6Au_3 surface is the most favorable among the three surfaces.

3. RESULTS AND DISCUSSION

3.1. Structure and Adsorption Energy of Reaction Intermediates. The adsorption energy (E_{ads}) is calculated as follows:

$$E_{ads} = E_{adsorbate/slab} - E_{(slab)} - E_{(adsorbate)}$$

where $E_{(slab)}$, $E_{(adsorbate)}$, and $E_{(adsorbate/slab)}$ are the total energies of the slab surface, the free adsorbate, and the slab surface with the adsorbate in the equilibrium state, respectively. With this definition, more negative values reflect the strong interaction of adsorbed species with the surface.

In this section, the adsorptions of all possible species involved in the reaction pathways of HCOOH oxidation have been considered over different adsorption sites of Pt(111) and three PtAu(111) surfaces. Figure 2 presents the most stable adsorption configurations obtained from our calculations, and Table 1 lists the corresponding adsorption energies and the preferential adsorption sites on Pt(111) and three PtAu(111) surfaces.

3.1.1. Formic Acid (HCOOH) Adsorption. HCOOH has two isomers: *trans*-HCOOH and *cis*-HCOOH. Our calculated results show that *trans*-HCOOH in the gas phase is more stable than *cis*-HCOOH in the gas phase; moreover, the interaction of *trans*-HCOOH with Pt(111) surface is stronger than *cis*-HCOOH, and the corresponding adsorption energies are −0.51 (−0.51[68]) and −0.41 eV, respectively.

For all four surfaces, the adsorption configurations of *trans*-HCOOH with the carbonyl oxygen adsorbed at the top Pt atom and OH group pointing down toward the surface are the most stable. Moreover, the formed Pt−O bond length range is between 2.349 and 2.410 Å; the most stable configurations correspond to the adsorption energies of −0.52 to −0.40 eV. Thus, the adsorption of *trans*-HCOOH is taken as the initial state of HCOOH oxidation on Pt(111) and three PtAu(111) surfaces. The geometrical configuration and adsorption energy agree with the reported results for HCOOH adsorption on Pt(111), PdAu(111), Pd(111), and Ni(111) surfaces.[15,62,69]

3.1.2. Formate (HCOO) Adsorption. The formate (HCOO) is formed through the O−H bond breaking of HCOOH; moreover, HCOO has been experimentally confirmed as a reactive intermediate in the direct pathway of HCOOH oxidation.[53,61,70,71] There are two adsorption modes for HCOO species: one is that only one oxygen atom binds with the surface, which is denoted as the monodentate isomer (mono-HCOO), and the other is that both oxygen atoms bind with the surface, which is denoted as the bidentate isomer (bi-HCOO).

Our results show that Pt distribution on Au(111) surface can affect the stability and geometry of HCOO species. Mono-HCOO species adsorbed at a top Pt atom with the corresponding adsorption energies of −1.77, −1.75, −1.75, and −1.68 eV on Pt(111), Pt ML, Pt_6Au_3, and Pt_3Au_6, respectively. Moreover, bi-HCOO is more stable than mono-HCOO, and the corresponding adsorption energies are −2.36 (−2.31[72]), −2.31, −2.32, and −2.07 eV on Pt(111), Pt ML, Pt_6Au_3, and Pt_3Au_6, respectively.

For bi-HCOO, due to the η^1-O-η^1-O configuration at the bridge site, it is noted that the adsorption energy of HCOO is closely related to the geometrical arrangements of Pt. As compared to Pt(111), Pt ML and Pt_6Au_3 show similar adsorption energies (−2.31 and −2.32 eV); two Pt−O bonds are slightly longer than these on Pt(111) surface. However, on

DOI: 10.1021/acs.jpcc.5b10831
J. Phys. Chem. C 2016, 120, 2234−2246

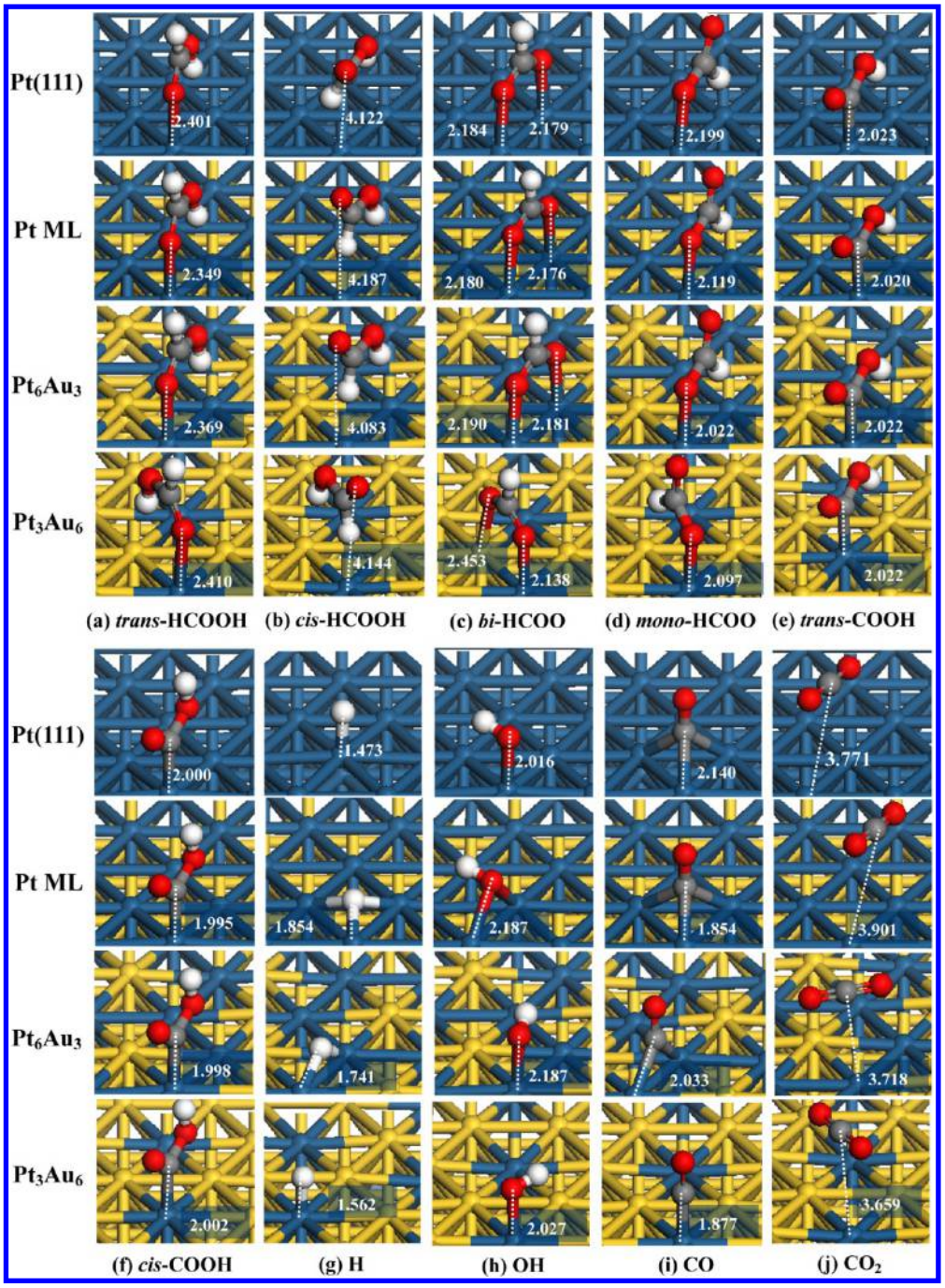

Figure 2. Most stable adsorption configurations of all possible species involved in HCOOH oxidation on Pt(111) and three PtAu(111) surfaces. The Pt, Au, C, H, and O atoms are shown as blue, yellow, gray, white, and red balls, respectively. Bond lengths are in angstroms.

Pt_3Au_6 surface, bi-HCOO adsorbed at the Pt−Au bridge site has only an adsorption energy of −2.07 eV due to the weak interaction between Au and O atoms, which is similar to the adsorption configuration reported on Pt-decorated Au(100) surface[68] and Pd-decorated Au(111) surface[15] due to the unavailability of the first neighboring Pt or Pd pair, respectively.

3.1.3. Carboxyl (COOH) Adsorption. Two isomers for carboxyl (COOH) exist: *trans*-COOH and *cis*-COOH. Our results show that the COOH species prefers to adsorb at the top Pt atom via its C atom on four surfaces regardless of the *trans*- or *cis*-structure.

trans-COOH has the adsorption energies of −2.63, −2.68, −2.63, and −2.55 eV on Pt(111), Pt ML, Pt_6Au_3, and Pt_3Au_6 surfaces, respectively, which are larger than those of *cis*-COOH with the corresponding adsorption energies of −2.58, −2.58, −2.55, and −2.51 eV, respectively. This result shows that the interactions of *trans*-COOH with Pt(111) and three PtAu(111) surfaces are stronger than those of *cis*-COOH; meanwhile, *trans*-COOH in the gas phase is found to be more stable than *cis*-COOH in the gas phase. The studies by Grabow and co-workers[72] have shown that *trans*-COOH adsorbed on Pt(111) surface is more stable by 0.16 eV than *cis*-COOH, and COOH intermediate binds through its C atom to a top Pt site of Pt(111), which agrees with our calculated results.

3.1.4. Other Reaction Intermediates. The adsorption energies of atomic H on Pt(111), Pt ML, Pt_6Au_3, and Pt_3Au_6

DOI: 10.1021/acs.jpcc.5b10831
J. Phys. Chem. C 2016, 120, 2234−2246

Table 1. Adsorption Sites and Adsorption Energies (E_{ads}/eV) of the Most Stable Adsorption Configurations for the Adsorbed Species Involved in HCOOH Oxidation on Pt(111) and Three PtAu(111) Surfaces

	Pt(111)		Pt ML		Pt_6Au_3		Pt_3Au_6	
species	sites	E_{ads}	sites	E_{ads}	sites	E_{ads}	sites	E_{ads}
trans-HCOOH	top	−0.51	top	−0.52	top-Pt	−0.50	top-Pt	−0.40
cis-HCOOH	top	−0.41	top	−0.51	top-Pt	−0.49	top-Pt	−0.46
bi-HCOO	bridge	−2.36	bridge	−2.31	Pt−Pt bridge	−2.32	Pt−Au bridge	−2.07
mono-HCOO	top	−1.77	top	−1.75	top-Pt	−1.75	top-Pt	−1.68
trans-COOH	top	−2.63	top	−2.68	top-Pt	−2.63	top-Pt	−2.55
cis-COOH	top	−2.58	top	−2.58	top-Pt	−2.55	top-Pt	−2.51
H	top	−2.79	fcc	−2.95	Pt−Pt bridge	−2.81	top-Pt	−2.76
OH	top	−2.31	bridge	−2.32	top-Pt	−2.28	top-Pt	−2.30
CO	fcc	−1.74	fcc	−2.02	Pt−Pt bridge	−1.78	top-Pt	−1.73
CO_2		−0.16		−0.16		−0.15		−0.16

Table 2. Possible Elementary Reactions Involved in HCOOH Oxidation on Pt(111) and Three PtAu(111) Surfaces Together with the Activation Energies (E_a/eV) and Reaction Energies (ΔH/eV)

	elementary reactions		Pt(111)	Pt ML	Pt_6Au_3	Pt_3Au_6
TS1	*trans*-HCOOH → bi-HCOO + H	E_a	0.91	0.89	0.85	1.37
		ΔH	0.18	0.12	0.24	0.53
TS2-1	bi-HCOO → mono-HCOO	E_a	1.11	0.94	0.94	0.62
		ΔH	0.59	0.56	0.57	0.39
TS2-2	mono-HCOO → CO_2 + H	E_a	0.01	0.01	0.02	1.06
		ΔH	−1.03	−1.05	−1.11	−0.94
TS3-1	*trans*-HCOOH → *cis*-HCOOH	E_a	0.81	0.78	0.77	0.73
		ΔH	0.29	0.20	0.20	0.13
TS3-2	*cis*-HCOOH → *trans*-COOH + H	E_a	0.69	0.73	0.78	0.90
		ΔH	−0.47	−0.59	−0.39	−0.07
TS4	*trans*-COOH → CO_2 + H	E_a	0.86	0.81	0.81	1.30
		ΔH	0.05	0.09	−0.03	0.11
TS5	*trans*-COOH → CO + OH	E_a		1.71	1.07	2.07
		ΔH		0.40	0.51	1.54
TS5-1	*trans*-COOH → *cis*-COOH	E_a	0.55			
		ΔH	0.12			
TS5-2	*cis*-COOH → CO + OH	E_a	1.24			
		ΔH	0.43			

surfaces are −2.79 (−2.78[73] and −2.71[72]), −2.95, −2.81, and −2.76 eV, respectively; the corresponding preferable adsorption sites are the top Pt site on Pt(111) and Pt_3Au_6 surface, the 3-fold fcc site on Pt ML surface, and the Pt−Pt bridge site on Pt_6Au_3 surface, respectively.

Hydroxyl (OH) prefers to adsorb at the Pt−Pt bridge site on Pt ML, and the top sites on Pt(111), Pt_6Au_3, and Pt_3Au_6 surfaces; the corresponding adsorption energies are −2.32, −2.31, −2.28, and −2.30 eV, respectively.

Carbon monoxide (CO) binds through its C atom with the C−O bond oriented perpendicular to the surface. It binds preferentially to the 3-fold fcc sites on Pt(111) and Pt ML surfaces, the Pt−Pt bridge site on Pt_6Au_3 surface, and the top Pt site on Pt_3Au_6 surface; the corresponding adsorption energies are −1.74 (−1.82[73]), −2.02, −1.78, and −1.73 eV, respectively. Obviously, the interaction of CO with Pt ML surface is much stronger than with the other three surfaces, which reminds us that when CO is formed, Pt ML surface may be seriously poisoned during the DFAFC reaction, because all catalytic active sites will be blocked by the adsorbed CO.[68]

Carbon dioxide (CO_2) interacts weakly with Pt(111) and three PtAu(111) surfaces; the corresponding adsorption energies are −0.15 or −0.16 eV. For all adsorption sites, CO_2 is far from the surface, and keeps its gas-phase linear geometry; CO_2 exhibits very weak site preference.

The above results show that all species involved in HCOOH oxidation, besides CO_2 and HCOOH, are found to be strongly bound to Pt(111) and three PtAu(111) surfaces. As compared to Pt(111) surface, both Pt ML and Pt_6Au_3 surfaces have few effects on the adsorption of *trans*-HCOOH. However, for Pt_3Au_6 surface, due to the decreased availability of adjacent Pt atoms over PtAu(111) surface, the interactions of Pt_3Au_6 surface with *trans*-HCOOH, HCOO, and COOH intermediates are weaker than with the other three surfaces, suggesting that the low loading of Pt on PtAu surfaces will reduce the stability of adsorbed species. Up to now, previous DFT calculations showed that the d-band of Pt on PtAu surfaces has changed due to the higher electronegativity of Au than Pt,[74,75] which is also confirmed by the experimentally high-resolution XPS data.[76] Meanwhile, because the lattice constant of Au is larger than that of Pt, the alloy property of Pt and Au results in a tensile strain, and both effects result in the stronger adsorption ability of adsorbed species on Pt than that on Au.

3.2. HCOOH Oxidation. As mentioned above, HCOOH oxidation occurs via a dual pathway mechanism consisting of the direct and indirect pathways. The direct pathway involves HCOOH oxidation to CO_2 without the participation of CO

DOI: 10.1021/acs.jpcc.5b10831
J. Phys. Chem. C 2016, 120, 2234−2246

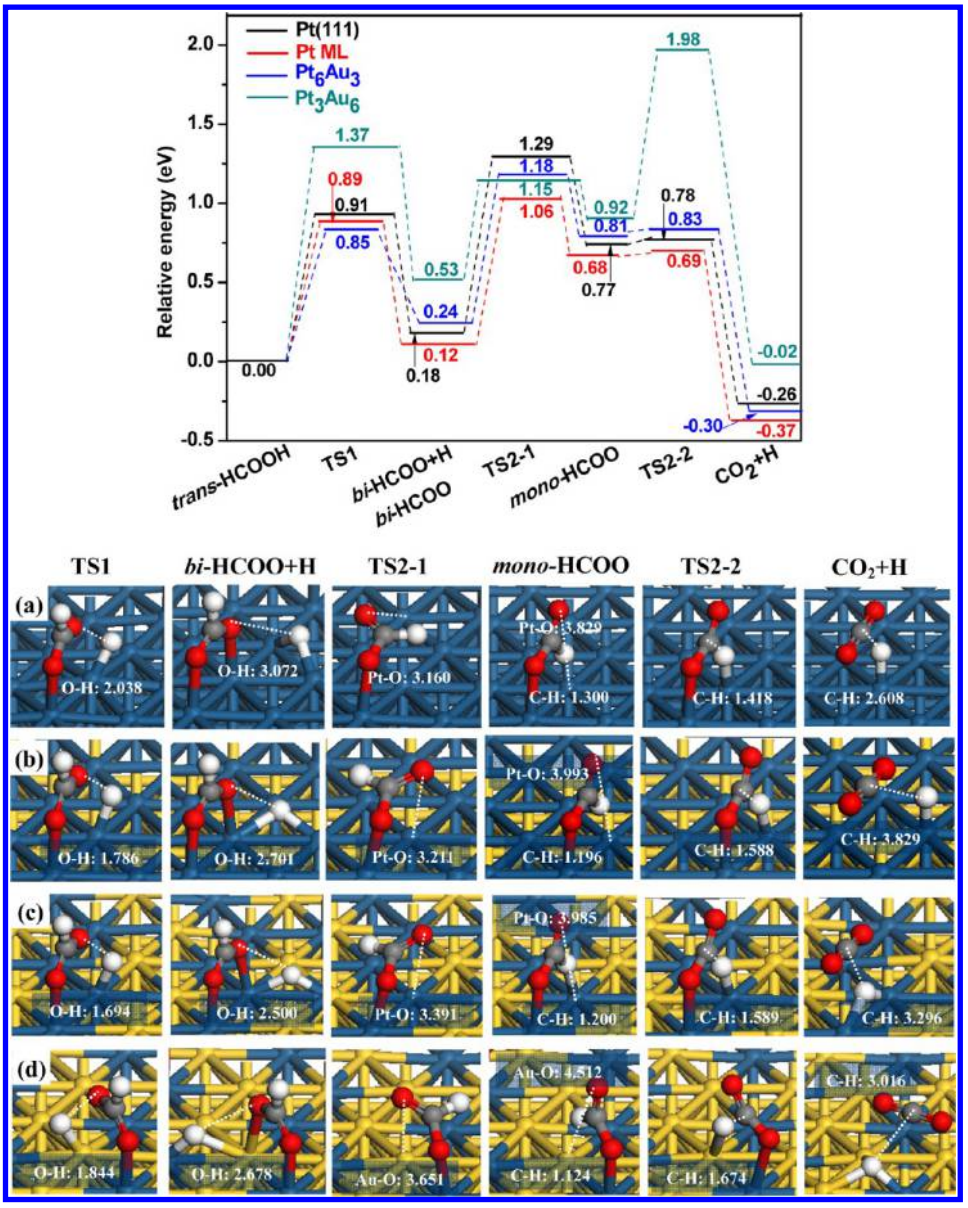

Figure 3. Potential energy profile for HCOOH dehydrogenation via HCOO intermediate in CO_2 pathway together with the initial states, transition states, and final states on (a) Pt(111) surface, (b) Pt ML, (c) Pt_6Au_3, and (d) Pt_3Au_6. Bond lengths are in angstroms. See Figure 2 for color coding.

species, which is denoted as CO_2 pathway; the indirect pathway features the adsorbed CO as the intermediate, denoted as CO pathway. Here, we have calculated the activation barrier (E_a) and reaction energy (ΔH) of all possible elementary steps in the above two pathways, as listed in Table 2, and the corresponding potential energy profiles are presented in Figures 3–5.

HCOOH oxidation via CO_2 pathway can proceed through the C–H or O–H bond cleavage of HCOOH, respectively, in which Pathway I starts from the O–H bond scission via the formate intermediate (HCOO), and Pathway II goes through the C–H bond cleavage via the carboxyl intermediate (COOH). Initially, the adsorption mode of *trans*-HCOOH is taken as the initial state of HCOOH oxidation on Pt(111) and three PtAu(111) surfaces.

3.2.1. CO_2 Pathway via HCOO Intermediate. Along Pathway I, as shown in Figure 3, we can found that the H atom of OH group can be removed from HCOOH via the transition state TS1, which have similar activation barriers of 0.91, 0.89, and 0.85 eV on Pt(111), Pt ML, and Pt_6Au_3 surfaces, respectively, and the reaction is endothermic with the reaction energy of 0.12–0.24 eV. However, this dehydrogenation process that occurred on Pt_3Au_6 surface is endothermic by 0.53 eV with a relatively high activation barrier of 1.37 eV, which means that the O–H bond cleavage of HCOOH has more difficulty occurring on Pt_3Au_6 surface than the other three surfaces; this result may attribute to the "ligand effect". Pt_3Au_6 surface shows the lower reactivity for the adsorption of HCOO and H in the final state (FS), in which both HCOO and H species are adsorbed at two Pt–Au bridge sites, and the interaction between H/C and Au atoms is weaker than that between H/C and Pt atoms; as a result, the O–H bond scission of HCOOH is energetically unfavorable on Pt_3Au_6 surface. Therefore, we can obtain that the contiguous Pt atomic ensemble makes the O–H bond cleavage of HCOOH more favorable on PtAu electrode during HCOOH oxidation. On the other hand, Pt_3Au_6 surface is less reactive than the pure Pt(111) surface for the O–H bond scission of HCOOH; however, Pt

DOI: 10.1021/acs.jpcc.5b10831
J. Phys. Chem. C 2016, 120, 2234–2246

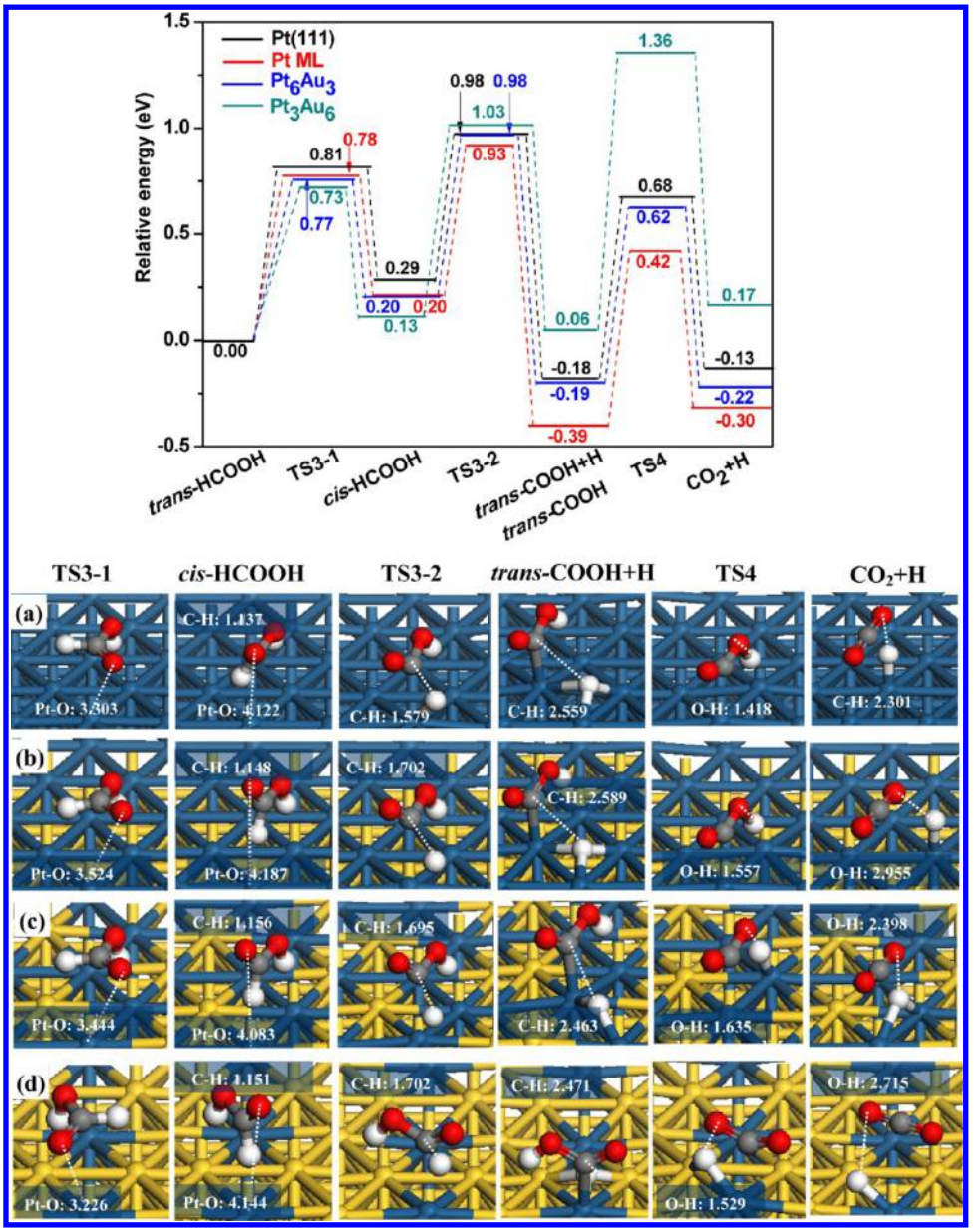

Figure 4. Potential energy profile for HCOOH dehydrogenation via COOH intermediate in CO_2 pathway together with the initial states, transition states, and final states on (a) Pt(111) surface, (b) Pt ML, (c) Pt_6Au_3, and (d) Pt_3Au_6. Bond lengths are in angstroms. See Figure 2 for color coding.

ML and Pt_6Au_3 surfaces can present a chemical reactivity similar to that of the pure Pt(111) surface.

After the first reaction (HCOOH → HCOO + H), the resulting HCOO intermediate is adsorbed at the bridge site in a bi-HCOO mode. Starting from bi-HCOO, interestingly, our results show that for bi-HCOO direct dissociation into CO_2 and H species, this reaction first needs to go through a metastable intermediate mono-HCOO, followed by the C−H bond cleavage to form CO_2 and H species. Thus, as shown in Figure 3, bi-HCOO is first converted into mono-HCOO via the transition state **TS2-1** with one Pt−O bond cleavage; subsequently, mono-HCOO dehydrogenates into CO_2 and H species via the transition state **TS2-2**.

On Pt(111) surface, the conversion from bi-HCOO to mono-HCOO is the rate-limiting step, which needs to overcome a relative high activation barrier of 1.11 eV, and then mono-HCOO can be easily dehydrogenated to CO_2 and H species with a quite low activation barrier of 0.01 eV; the overall activation barrier of HCOO dehydrogenation into CO_2 is 1.11 eV with an reaction energy of −0.44 eV on Pt(111) surface, which agrees with the previous DFT results by Gabow et al.[72] with E_a = 1.04 eV and ΔH = −0.35 eV.

Similarly, on Pt ML and Pt_6Au_3 surfaces, bi-HCOO converts into mono-HCOO with the activation barrier of 0.94 eV, and then mono-HCOO can easily dehydrogenate into CO_2 with a quite low activation barrier of 0.01 and 0.02 eV, respectively. In contrast, on Pt_3Au_6 surface, bi-HCOO can easily convert to mono-HCOO with a low activation barrier of 0.62 eV; however, mono-HCOO dehydrogenation to CO_2 and H species needs to overcome a relative high activation barrier of 1.06 eV, which is the rate-limiting step.

3.2.2. CO_2 Pathway via COOH Intermediate. Along Pathway II, as shown in Figure 4, *trans*-HCOOH first needs to be converted into *cis*-HCOOH via the transition state **TS3-1** with the activation barrier of 0.73−0.81 eV on Pt(111) and three PtAu surfaces. Such a *cis*-HCOOH structure is identified

DOI: 10.1021/acs.jpcc.5b10831
J. Phys. Chem. C 2016, 120, 2234−2246

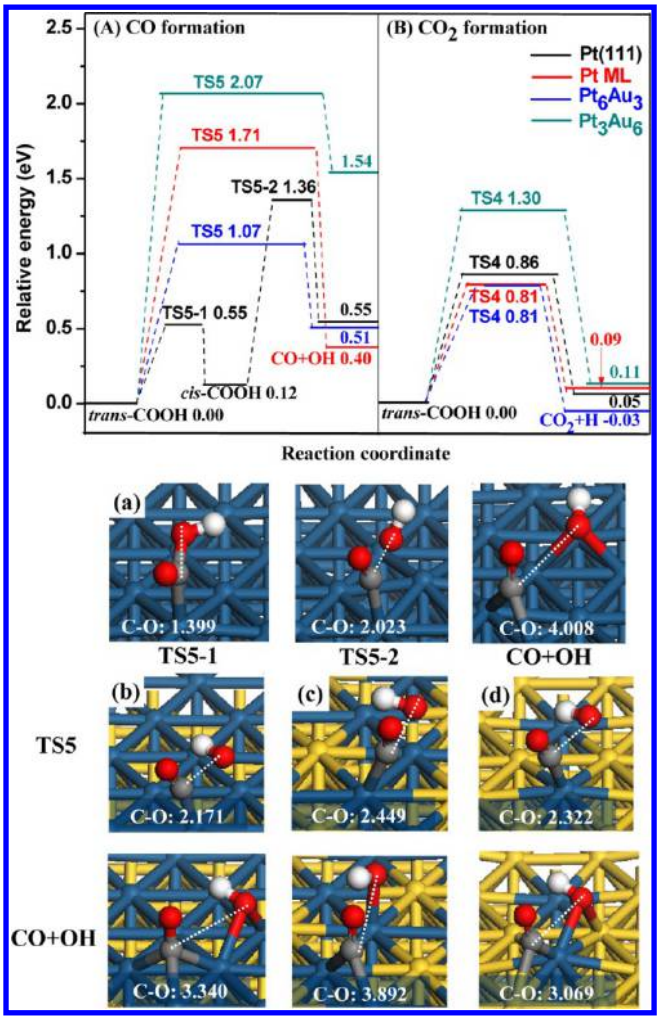

Figure 5. Comparison of potential energy diagram for (A) CO and (B) CO_2 formations from *trans*-COOH intermediate together with the initial states, transition states, and final states on (a) Pt(111) surface, (b) Pt ML, (c) Pt_6Au_3, and (d) Pt_3Au_6 surfaces, respectively. Bond lengths are in angstroms. See Figure 2 for color coding.

as the energetically most favorable precursor for the subsequent formation of CO and CO_2 species. The adsorbed *cis*-HCOOH is higher in energy than the most stable adsorbed state *trans*-HCOOH; however, it brings the carbonic hydrogen of HCOOH closer to the surface, which facilitates the C−H bond cleavage. As a result, *cis*-HCOOH can be dehydrogenated into *trans*-COOH and H species via the transition state **TS3-2** on Pt(111) and three PtAu(111) surfaces, in **TS3-2**; the corresponding distance between dissociated H and C atoms is elongated to about 1.700 Å.

On Pt(111), Pt ML, and Pt_6Au_3 surfaces, *cis*-HCOOH dehydrogenation to yield *trans*-COOH and H species has the activation barriers of 0.69, 0.73, and 0.78 eV, respectively. As compared to the above three surfaces, on Pt_3Au_6 surface, only one isolated Pt site is available for the coadsorption of H and COOH species, which shows the low reactivity for the coadsorption of COOH and H in the final state due to the weaker interaction between Au and H atoms than that between Pt and H atoms; thus, the activation barrier for the C−H bond cleavage of *cis*-HCOOH to *trans*-COOH and H species is increased to 0.90 eV.

As displayed in Figure 4, the second dehydrogenation step (*trans*-COOH → CO_2 + H) occurs via the transition state **TS4** and leads to CO_2 and H species. This reaction occurred over four surfaces that are nearly thermoneutral, and the reaction coordinate is simple: the dissociated H atom that is already oriented toward a surface top Pt site breaks the C−H bond with the remaining CO_2 molecule. In **TS4**, the OCO fragment is away from the surface with a O═C═O angle of about 141°, and the O−H bond is elongated to 1.418−1.635 Å. On Pt(111) surface, this elementary reaction has an activation barrier of 0.86 eV, which is close to the previous reported values on Pt(111) surface, such as 0.89 eV by Qi et al.[77] and 0.78 eV by Gabow et al.[72] Similarly, on Pt ML and Pt_6Au_3 surfaces, this elementary reaction has an activation barrier of 0.81 eV. However, on Pt_3Au_6 surface, this reaction has a high activation barrier of 1.30 eV; the cause may be a small amount of doping Pt content over Au(111) surface. Therefore, the contiguous Pt atomic ensemble on Au(111) surface is still favorable for the O−H bond cleavage of *trans*-COOH.

3.2.3. Brief Summary about CO_2 Pathway. With respect to *trans*-HCOOH, as shown in Figure 3, the highest barriers of CO_2 formation via HCOO intermediate are 1.29, 1.06, 1.18, and 1.98 eV on Pt(111), Pt ML, Pt_6Au_3, and Pt_3Au_6 surfaces, respectively; the corresponding reaction energies are −0.26, −0.37, −0.30, and −0.02 eV, respectively, suggesting that, as compared to Pt(111) surface, Pt_3Au_6 surface has more difficulty catalyzing HCOOH oxidation to form CO_2 via HCOO intermediate, whereas Pt ML and Pt_6Au_3 surfaces are more favorable than Pt(111) surface.

On the other hand, as shown in Figure 4, the highest barriers of CO_2 formation via COOH intermediate are 0.98, 0.93, 0.98, and 1.36 eV on Pt(111), Pt ML, Pt_6Au_3, and Pt_3Au_6 surfaces, respectively; the corresponding reaction energies are −0.13, −0.30, −0.22, and 0.17 eV, respectively, indicating that Pt ML surfaces are more favorable for CO_2 formation than Pt(111) surface, and Pt_6Au_3 surface exhibits a catalytic activity similar to that of Pt(111) surface, whereas Pt_3Au_6 surface has more difficulty catalyzing HCOOH oxidation to form CO_2 via COOH intermediate.

The above results show that, as compared to Pt(111) surface, only an appropriate amount of Pt atomic ensemble over Au(111) surface can exhibit the high or similar catalytic activity toward CO_2 formation from HCOOH oxidation via HCOO and COOH intermediates, such as Pt ML and Pt_6Au_3 surfaces, which is a realizable structure that is not only efficient in the utilization of Pt but also highly active for HCOOH oxidation to CO_2. In the final state, CO_2 is far from the surface; however, H atom remains over the surface, and may interact with the adjacent H atoms to form H_2.

3.2.4. CO Pathway. For the poisoning species CO formation, our results show that if HCOO intermediate wants to form CO, HCOO first needs to convert into COOH through the hydrogen transfer from C to O atom, then the C−OH bond cleavage of COOH leads to CO; however, HCOO conversion into COOH is much more difficult than HCOO dehydrogenation into CO_2, as HCOO prefers to be dehydrogenated into CO_2 via the C−H bond cleavage rather than being converted into COOH via hydrogen transfer; therefore, the poisoning species CO is dominantly produced by the C−OH bond cleavage of COOH intermediate. On the other hand, previous studies[11,53,69] have shown that the adsorbed HCOOH also can first break its C−OH bond to form CHO and OH species, then the C−H bond

DOI: 10.1021/acs.jpcc.5b10831
J. Phys. Chem. C 2016, 120, 2234−2246

scission of CHO species leads to the formation of CO; however, these reported studies have shown that the CO pathway via COOH intermediate is the energetically most favorable. For example, Qi et al.[11] have explored the mechanism details for the elementary steps of HCOOH decomposition on Pt(111) and PtAg(111) surfaces by performing DFT calculations, which consider three possible pathways of HCOOH decomposition to CO on Pt(111) and PtAg(111) surfaces, including COOH and CHO intermediates, and the results show that the COOH intermediate pathway is the most favorable. Zhang and co-workers[69] have reported the reaction of HCOOH → CHO + OH → CO + H_2O on Pd(111) surface, suggesting that this pathway is less favorable than HCOOH → COOH + H → CO + H_2O. Singh et al.[53] combined theoretical and experimental methods to investigate HCOOH decomposition on the Au(111), Au(100), and Au(211) surfaces, and the calculated activation barriers show that the decomposition of HCOOH to yield CHO and OH is significantly higher than the HCOO and COOH formation steps. As a result, in this study, only one reaction of COOH → CO + OH has been considered to investigate CO formation pathway, as shown in Figure 5.

As mentioned before, the C−H bond cleavage of HCOOH leads to *trans*-COOH intermediate, and then starting from *trans*-COOH, on Pt(111) surface, CO formation involves two elementary reactions: first, *trans*-COOH converts into *cis*-COOH with a small activation barrier of 0.55 eV via the transition state **TS5-1**; then *cis*-COOH breaks its C−OH bond via the transition state **TS5-2** to form CO and OH species; in **TS5-2**, the C−OH distance has been stretched to 2.023 Å (2.240[72] Å), and this elementary step has an activation barrier of 1.24 eV. Thus, the overall activation barrier of *trans*-COOH intermediate dehydrogenation into CO is 1.36 eV with an reaction energy of 0.55 eV on Pt(111) surface, which agrees with the previous DFT results by Gao et al.[24]

Different from the pure Pt(111) surface, on PtAu(111) surfaces, *trans*-COOH can directly break its C−OH bond to form CO via the transition state **TS5** rather than being first converted into *cis*-COOH, followed by CO formation. Moreover, the activation barrier for the C−OH bond breaking of *trans*-COOH strongly depends on the Pt atomic ensemble over PtAu surfaces. On Pt ML and Pt_3Au_6 surfaces, CO formation has an activation barrier of 1.71 and 2.07 eV, respectively, the values of which are higher than that (1.36 eV) on Pt(111); however, on Pt_6Au_3 surface, the C−OH bond cleavage of COOH only needs an activation barrier of 1.07 eV. Meanwhile, CO formation reaction is endothermic by 0.55, 0.40, and 0.51 eV on Pt(111), Pt ML, and Pt_6Au_3, respectively; especially, for Pt_3Au_6 surface, this reaction is highly endothermic by 1.54 eV, indicating it is a strong endothermic process.

On the other hand, on Pt(111) surface, four contiguous Pt atoms are involved to stabilize two segments CO and OH species adsorbed at two Pt−Pt bridge sites; on Pt ML surface, CO and OH species are adsorbed at the 3-fold fcc and the Pt−Pt bridge sites, respectively; on Pt_6Au_3 surface, CO is adsorbed at the Pt−Pt bridge site, and OH is adsorbed at the top Pt site; however, on Pt_3Au_6 surface, CO formation mainly focuses on the single top Pt atom, as both CO and OH species are adsorbed at two adjacent Pt−Au bridge sites, in which the interaction of adsorbed species with Au is more weaker than that with Pt; further, all configurations also indicate that Pt sites are the reaction active center.[61]

Thus, Pt_3Au_6 surface without the continuous Pt atoms over Pt-decorated Au(111) surface can effectively inhibit CO formation. Moreover, the studies by Cuesta et al.[78] have shown that HCOOH oxidation to CO requires at least three adjacent Pt atoms. The cyclic voltammetry results by Chen et al.[14] have proved that the CO pathway may be suppressed in an appropriate ratio between Pt and Au (Pt:Au ≤ 1). Recent studies[61] have also demonstrated that the small Pt ensembles can facilitate the dehydrogenation of HCOOH oxidation through CO_2 pathway due to the higher activation barrier of CO formation. As mentioned above, our results about the decreased catalytic activity of Pt_3Au_6 surface without the continuous Pt atoms over PtAu(111) surface toward CO formation agree well with an ensemble effect, in which the decreased availability of adjacent Pt atoms over PtAu surface can suppress the CO poisoning of the catalyst.

3.3. General Discussion. As mentioned above, the detailed mechanism of HCOOH oxidation to CO_2 or CO species on Pt(111) and three PtAu(111) surfaces has been systematically examined. As shown in Figure 6, first, two pathways of CO_2 formation are discussed, one is HCOO pathway (Pathway I) formed by the O−H bond cleavage of HCOOH, in which two reactions of HCOOH → HCOO + H and HCOO → CO_2 + H occur, while the latter needs the conversion of bi-HCOO to mono-HCOO, followed by the dehydrogenation into CO_2 and H species; the other is COOH pathway (Pathway II) formed by the C−H bond cleavage of HCOOH, in which two reactions of HCOOH → COOH + H and COOH → CO_2 + H exist; the former requires the conversion of the stable state *trans*-HCOOH to a metastable state *cis*-HCOOH, which can facilitate the C−H bond cleavage of HCOOH. Second, starting from COOH intermediates, only one pathway of CO formation exists via the C−OH bond cleavage, COOH → CO + OH.

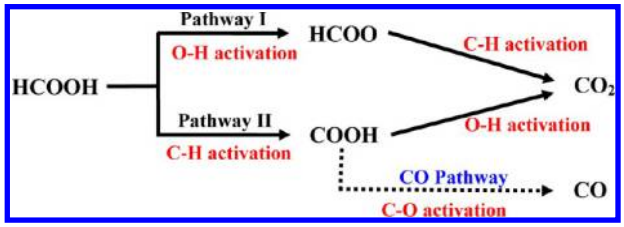

Figure 6. Schematic diagram of the reaction pathways for HCOOH oxidation.

3.3.1. Effect of Pt Atomic Ensemble on HCOOH Oxidation. Previous studies by Yuan et al.[79] have shown that the activation barrier of CH_3OH oxidation depends on proper placement of two segments in the transition state, and thus the activation barrier is more sensitive to the atomic distribution of alloy surface, that is, the ensemble effects; moreover, the drastically different activities of Au and Pt sites provide ample potential to tune the reactivity and selectivity of catalysts through non-CO pathway leading to the high H productivity in the direct methanol fuel cells. In this study, our results show that Pt-decorated Au(111) surfaces, Pt ML and Pt_6Au_3, exhibit a chemical reactivity similar to that of the pure Pt(111) surface toward the initial HCOOH dehydrogenation.

As compared to Pt(111) surface, the lower activation barriers of CO_2 formation on Pt ML and Pt_6Au_3 indicate that Pt-decorated Au catalysts with a proper arrangement of Au and Pt sites can exhibit a high or similar catalytic activity toward the C−H or O−H bond cleavage of HCOO and COOH

DOI: 10.1021/acs.jpcc.5b10831
J. Phys. Chem. C 2016, 120, 2234−2246

intermediates, respectively, whereas the Pt_3Au_6 surface is less reactive for these reactions than the other three surfaces. The cause may be attributed to that a larger Pt atomic ensemble is required to activate the O−H and C−H bonds, and the nearby Pt atoms are favorable for stabilizing the transition state (TS) and final state (FS); however, Pt_3Au_6 surface has only three isolated Pt atoms incorporated into Au(111) without the nearby Pt atoms, which shows a very low chemical reactivity for HCOOH oxidation. Therefore, among Pt-decorated Au(111) surfaces, for HCOOH oxidation, it is noted that Pt sites are the reaction active center; moreover, the catalytic activity of PtAu(111) surface toward HCOOH oxidation is obviously dependent on the atomic ensemble of the reaction active center.

On the other hand, as far as we know, two critical factors exist, train effects and ligand effect, which contribute to the modification of the electronic properties of a metal in a bimetallic surface.[80] Pt monolayer on Au lattice is under a tensile strain because of a larger lattice constant of Au than that of Pt, which has been verified by Li et al.[81] in the experiment, in which a significant enhancement in the catalytic has been associated with the tensile strain. Moreover, the strain effect results in an increase in d-band center of Pt atoms in monolayer, and the ligand effect arising from the heterometallic bonding between Pt and Au also increases d-band energy, both effects leading to the stronger adsorption of CO and OH on Pt ML surface.[80,82] In addition, Ahn et al.[83] have suggested that the positive influence of a Pt monolayer has largely been attributed to either strain or ensemble effects; Kristian and co-workers[84] also have proposed that the ensemble effect and possibly electronic effect may increase the reactivity of the Pt entities on Au substrate. Thus, we consider that these effects including the strain effect, ligand effect, and ensemble effect can contribute to the enhanced selectivity toward CO_2 formation for HCOOH decomposition on Pt ML surface.

3.3.2. Selectivity between CO_2 and CO. Starting from *trans*-COOH species, the activation barrier of the rate-limiting step for CO formation via the C−OH bond cleavage is always higher than that for CO_2 formation via the O−H bond cleavage on Pt(111) and three Pt-decorated Au(111) surfaces, indicating that CO_2 is the dominant product of HCOOH oxidation.

Interestingly, to better understand the modified reaction behavior of bimetallic PtAu catalysts as compared to monometallic Pt catalysts, it is necessary to quantify the selectivity between CO_2 and CO on Pt(111) and three PtAu(111) surfaces; the effective barrier difference between CO_2 and CO formations is used a descriptor. In principle, the higher barrier difference represents the higher selectivity of CO_2 and the lower selectivity of CO.

As shown in Figure 5, with respect to *trans*-COOH species, our calculated barrier differences between CO_2 and CO formations are 0.50, 0.90, 0.26, and 0.77 eV on Pt(111), Pt ML, Pt_6Au_3, and Pt_3Au_6 surfaces, respectively; obviously, Pt ML and Pt_3Au_6 surfaces exhibit the higher selectivity of HCOOH oxidation to CO_2, as well as the lower selectivity of HCOOH oxidation to CO, which implies that CO pathway can not easily compete with CO_2 pathway during HCOOH oxidation on Pt ML and Pt_3Au_6 surfaces. The above results suggest that the catalytic selectivity of PtAu(111) surface toward HCOOH oxidation also obviously depends on the atomic ensemble of the reaction active center.

Overall, Pt-decorated Au(111) surface is efficient for the dehydrogenation of HCOOH oxidation to CO_2, and shows an inhibiting effect to the dehydration of HCOOH to CO. Especially, Pt ML surface exhibits the highest catalytic activity and selectivity toward the dehydrogenation of HCOOH oxidation, and can highly suppress the formation of poisonous species CO; a Pt skin consisting of 1.0 monolayer Pt on a Au substrate is a realizable structure, which is not only efficient to utilize Pt, but also is highly active and selective for HCOOH oxidation to CO_2.

On the other hand, experimental studies by Kristian et al.[85] have synthesized an Au core with Pt shell structure to improve Pt utilization, which exhibits a higher specific activity as compared to the conventional Pt/C using TEM, UV−vis, and cyclic voltammetry; our Pt ML surface model in this study is similar to this Pt_{shell}−Au_{core} structure, in which a Pt overlay is exposed in the catalytic reaction, suggesting that Pt ML surface can exhibit the high selectivity to CO_2 formation during HCOOH decomposition. Kim et al.[86] have experimentally presented the catalytic activity variations of HCOOH oxidation on Pt deposits over Au(111) surface, suggesting that small and thin layer Pt deposits are advantageous to HCOOH oxidation. Li et al.[81] have synthesized the electrocatalysts consisting of one Pt monolayer placed on extended or nanoparticle surfaces, suggesting that Pt/Au(111) exhibits a factor of 7 activity increase in catalyzing methanol electrooxidation as compared to the pure Pt(111) surface. Meanwhile, Banerjee and co-workers[87] have reported that the electrochemical activity (HOR, MOR studies) of Au@Pt nanoparticles was found to be the highest for particles with two thick layer Pt's. As mentioned above, these experimental studies demonstrate that Pt ML surface can exhibit the high activity and selectivity toward HCOOH oxidation, which agrees with our calculated results.

Therefore, we can conclude that the enhanced catalytic activity and selectivity of bimetallic PtAu catalysts toward HCOOH oxidation should be attributed to their suppression to the dehydration reactions of HCOOH to CO, which is supported by the previous experimental results that the high catalytic activity of PtAu surface is caused by the increased selectivity toward HCOOH dehydrogenation.[51,52]

4. CONCLUSIONS

In summary, we have investigated the detailed mechanism for a dual pathway of HCOOH oxidation on Pt(111) and three PtAu(111) surfaces with different Pt atomic ensembles by performing DFT calculations. The adsorption energy of HCOOH is very close over different Pt atomic ensembles, but the activation of O−H and C−H bonds is related to the atomic arrangement of Au and Pt over PtAu(111) surface. Pt-decorated Au(111) surface is more active to catalyze HCOOH oxidation via CO_2 pathway rather than that via CO pathway, which explains well the experimental facts that PtAu bimetallic catalysts enhance the catalytic activity toward HCOOH oxidation and the ability of CO antipoisoning. The present insights reveal that the ensemble effects play a crucial role to tune the reactivity and selectivity of HCOOH oxidation due to the drastically different activities of Au and Pt sites, which may provide some information for the design and optimization of highly efficient Au-based catalysts used in DFAFC.

AUTHOR INFORMATION

Corresponding Authors

*Tel.: +86 351 6018239. Fax: +86 351 6041237. E-mail: zhangriguang@tyut.edu.cn, zhangriguang1981@163.com.

DOI: 10.1021/acs.jpcc.5b10831
J. Phys. Chem. C 2016, 120, 2234−2246

*E-mail: wangbaojun@tyut.edu.cn.

Notes

The authors declare no competing financial interest.

■ ACKNOWLEDGMENTS

This work is financially supported by the National Natural Science Foundation of China (nos. 21276003, 21476155, 21576178, and 21276171), the Natural Science Foundation of Shanxi Province (no. 2014011012-2), the Program for the Top Young Academic Leaders of Higher Learning Institutions of Shanxi, and the Top Young Innovative Talents of Shanxi.

■ REFERENCES

(1) Yu, X. W.; Pickup, P. G. Recent Advances in Direct Formic Acid Fuel Cells (DFAFC). *J. Power Sources* **2008**, *182*, 124−132.
(2) Kristian, N.; Yan, Y.; Wang, X. Highly Efficient Submonolayer Pt-Decorated Au Nano-Catalysts for Formic Acid Oxidation. *Chem. Commun.* **2008**, 353−355.
(3) Ha, S.; Larsen, R.; Masel, R. I. Performance Characterization of Pd/C Nanocatalyst for Direct Formic Acid Fuel Cells. *J. Power Sources* **2005**, *144*, 28−34.
(4) Huang, Y. J.; Zhou, X. C.; Liao, J. H.; Liu, C. P.; Lu, T. H.; Xing, W. Preparation of Pd/C Catalyst for Formic Acid Oxidation Using a Novel Colloid Method. *Electrochem. Commun.* **2008**, *10*, 621−624.
(5) Haan, J. L.; Masel, R. I. The Influence of Solution pH on Rates of an Electrocatalytic Reaction: Formic Acid Electrooxidation on Platinum and Palladium. *Electrochim. Acta* **2009**, *54*, 4073−4078.
(6) Zhang, L. L.; Lu, T. H.; Bao, J. C.; Tang, Y. W.; Li, C. Preparation Method of an Ultrafine Carbon Supported Pd Catalyst as an Anodic Catalyst in a Direct Formic Acid Fuel Cell. *Electrochem. Commun.* **2006**, *8*, 1625−1627.
(7) Uhm, S.; Chung, S. T.; Lee, J. Characterization of Direct Formic Acid Fuel Cells by Impedance Studies: In Comparison of Direct Methanol Fuel Cells. *J. Power Sources* **2008**, *178*, 34−43.
(8) Zhong, W. H.; Wang, R. Y.; Zhang, D. J.; Liu, C. B. Theoretical Study of the Oxidation of Formic Acid on the PtAu(111) Surface in the Continuum Water Solution Phase. *J. Phys. Chem. C* **2012**, *116*, 24143−24150.
(9) Wang, Y. Y.; Qi, Y. Y.; Zhang, D. J. New Mechanism of the Direct Pathway for Formic Acid Oxidation on Pd(111). *Comput. Theor. Chem.* **2014**, *1049*, 51−54.
(10) Yu, W. Y.; Mullen, G. M.; Flaherty, D. W.; Mullins, C. B. Selective Hydrogen Production from Formic Acid Decomposition on Pd-Au Bimetallic Surfaces. *J. Am. Chem. Soc.* **2014**, *136*, 11070−11078.
(11) Qi, Y. Y.; Gao, J.; Zhang, D. J.; Liu, C. B. Comparative Theoretical Study of Formic Acid Decomposition on PtAg(111) and Pt(111) Surfaces. *RSC Adv.* **2015**, *5*, 21170−21177.
(12) Zhang, S.; Shao, Y. Y.; Yin, G. P.; Lin, Y. H. Electrostatic Self-Assembly of a Pt-around-Au Nanocomposite with High Activity Towards Formic Acid Oxidation. *Angew. Chem., Int. Ed.* **2010**, *49*, 2211−2214.
(13) Adams, B. D.; Asmussen, R. M.; Ostrom, C. K.; Chen, A. Synthesis and Comparative Study of Nanoporous Palladium-Based Bimetallic Catalysts for Formic Acid Oxidation. *J. Phys. Chem. C* **2014**, *118*, 29903−29910.
(14) Chen, G. Q.; Li, Y. H.; Wang, D.; Zheng, L.; You, G. R.; Zhong, C. J.; Yang, L. F.; Cai, F.; Cai, J. X.; Chen, B. H. Carbon-Supported PtAu Alloy Nanoparticle Catalysts for Enhanced Electrocatalytic Oxidation of Formic Acid. *J. Power Sources* **2011**, *196*, 8323−8330.
(15) Yuan, D. W.; Liu, Z. R. Atomic Ensemble Effects on Formic Acid Oxidation on PdAu Electrode Studied by First-Principles Calculations. *J. Power Sources* **2013**, *224*, 241−249.
(16) Stevanović, S.; Tripković, D.; Tripkovic, V.; Minić, D.; Gavrilović, A.; Tripković, A.; Jovanović, V. M. Insight into the Effect of Sn on CO and Formic Acid Oxidation at PtSn Catalysts. *J. Phys. Chem. C* **2014**, *118*, 278−289.
(17) Solla-Gullon, J.; Montiel, V.; Aldaz, A.; Clavilier, J. Electrochemical and Electrocatalytic Behaviour of Platinum-Palladium Nanoparticle Alloys. *Electrochem. Commun.* **2002**, *4*, 716−721.
(18) Obradović, M. D.; Gojković, S. L. Pd Black Decorated by Pt Sub-Monolayers as an Electrocatalyst for the HCOOH Oxidation. *J. Solid State Electrochem.* **2014**, *18*, 2599−2607.
(19) Babu, P. K.; Kim, H. S.; Chung, J. H.; Oldfield, E.; Wieckowski, A. Bonding and Motional Aspects of CO Adsorbed on the Surface of Pt Nanoparticles Decorated with Pd. *J. Phys. Chem. B* **2004**, *108*, 20228−20232.
(20) Jiang, K.; Zhang, H. X.; Zou, S. Z.; Cai, W. B. Electrocatalysis of Formic Acid on Palladium and Platinum Surfaces: From Fundamental Mechanisms to Fuel Cell Applications. *Phys. Chem. Chem. Phys.* **2014**, *16*, 20360−20376.
(21) Zhang, K.; Wang, H. W.; Wang, C. Q.; Yang, B. B.; Ren, F. F.; Yang, P.; Du, Y. K. Facile Fabrication of PtCuAu Nanoparticles Modified Reduced Graphene Oxide with High Electrocatalytic Activity toward Formic Acid Oxidation. *Colloids Surf., A* **2015**, *467*, 211−215.
(22) Gao, W.; Song, E. H.; Jiang, Q.; Jacob, T. Revealing the Active Intermediates in the Oxidation of Formic Acid on Au and Pt(111). *Chem. - Eur. J.* **2014**, *20*, 11005−11012.
(23) Xu, J.; Yuan, D. F.; Yang, F. Y.; Mei, D.; Zhang, Z. B.; Chen, Y. X. On the Mechanism of the Direct Pathway for Formic Acid Oxidation at a Pt(111) Electrode. *Phys. Chem. Chem. Phys.* **2013**, *15*, 4367−4376.
(24) Gao, W.; Keith, J. A.; Anton, J.; Jacob, T. Oxidation of Formic Acid on the Pt(111) Surface in the Gas Phase. *Dalton Trans.* **2010**, *39*, 8450−8456.
(25) Osawa, M.; Komatsu, K.; Samjeské, G.; Uchida, T.; Ikeshoji, T.; Cuesta, A.; Gutiérrez, C. The Role of Bridge-Bonded Adsorbed Formate in the Electrocatalytic Oxidation of Formic Acid on Platinum. *Angew. Chem., Int. Ed.* **2011**, *50*, 1159−1163.
(26) Cho, J.; Lee, S.; Han, J.; Yoon, S. P.; Nam, S. W.; Choi, S. H.; Lee, K. Y.; Ham, H. C. Importance of Ligand Effect in Selective Hydrogen Formation via Formic Acid Decomposition on the Bimetallic Pd/Ag Catalyst from First-Principles. *J. Phys. Chem. C* **2014**, *118*, 22553−22560.
(27) Lee, S. Y.; Jung, N.; Cho, J.; Waszczuk, P.; Park, H. Y.; Ryu, J.; Jang, I.; Kim, H. J.; Cho, E.; Park, Y. H.; Ham, H. C.; Jang, J. H.; Yoo, S. J. Surface-Rearranged Pd_3Au/C Nanocatalysts by Using CO-Induced Segregation for Formic Acid Oxidation Reactions. *ACS Catal.* **2014**, *4*, 2402−2408.
(28) Yoo, S. J.; Zhao, Z. J.; Nørskov, J. K.; Studt, F. Effect of Boron Modifications of Palladium Catalysts for the Production of Hydrogen from Formic Acid. *ACS Catal.* **2015**, *5*, 6579−6586.
(29) Rice, C.; Ha, S.; Masel, R. I.; Waszczuk, P.; Wieckowski, A.; Barnard, T. Direct Formic Acid Fuel Cells. *J. Power Sources* **2002**, *111*, 83−89.
(30) Waszczuk, P.; Crown, A.; Mitrovski, S.; Wieckowski, A. Methanol and Formic Acid Oxidation on Ad-Metal Modified Electrodes. *Handbook of Fuel Cells*; John Wiley & Sons: Chichester, UK, 2003; Vol. 2, pp 635−651.
(31) Li, X. G.; Hsing, I. M. Electrooxidation of Formic Acid on Carbon Supported Pt_xPd_{1-x} (x = 0−1) Nanocatalysts. *Electrochim. Acta* **2006**, *51*, 3477−3483.
(32) Casado-Rivera, E.; Gál, Z.; Angelo, A. C. D.; Lind, C.; DiSalvo, F. J.; Abruña, H. D. Electrocatalytic Oxidation of Formic Acid at an Ordered Intermetallic PtBi Surface. *ChemPhysChem* **2003**, *4*, 193−199.
(33) Matsumoto, F.; Roychowdhury, C.; DiSalvo, F. J.; Abruña, H. D. Electrocatalytic Activity of Ordered Intermetallic PtPb Nanoparticles Prepared by Borohydride Reduction toward Formic Acid Oxidation. *J. Electrochem. Soc.* **2008**, *155*, B148−B154.
(34) Yu, X.; Pickup, P. G. Pb and Sb Modified Pt/C Catalysts for Direct Formic Acid Fuel Cells. *Electrochim. Acta* **2010**, *55*, 7354−7361.
(35) Tripković, A. V.; Gojković, S. L.; Popović, K. D.; Lović, J. D.; Kowal, A. Study of the Kinetics and the Influence of Bi_{Irr} on Formic Acid Oxidation at Pt_2 Ru_3/C. *Electrochim. Acta* **2007**, *53*, 887−893.

DOI: 10.1021/acs.jpcc.5b10831
J. Phys. Chem. C 2016, 120, 2234−2246

(36) Chen, W.; Kim, J.; Sun, S. H.; Chen, S. W. Composition Effects of FePt Alloy Nanoparticles on the Electro-Oxidation of Formic Acid. *Langmuir* **2007**, *23*, 11303−11310.
(37) Zhang, S.; Shao, Y. Y.; Yin, G. P.; Lin, Y. H. Facile Synthesis of PtAu Alloy Nanoparticles with High Activity for Formic Acid Oxidation. *J. Power Sources* **2010**, *195*, 1103−1106.
(38) Yu, Y. L.; Lim, K. H.; Wang, J. Y.; Wang, X. CO Adsorption Behavior on Decorated Pt@Au Nanoelectrocatalysts: A Combined Experimental and DFT Theoretical Calculation Study. *J. Phys. Chem. C* **2012**, *116*, 3851−3856.
(39) Schneider, U.; Busse, H.; Linke, R.; Castro, G.; Wandelt, K. Interaction Properties of Molecules with Binary Alloy Surfaces. *J. Vac. Sci. Technol., A* **1994**, *12*, 2069−2073.
(40) Sinfelt, J. H. *Bimetallic Catalysts: Discoveries, Concepts, and Applications*; Wiley: New York, 1983; Vol. 7, pp 15−17.
(41) Zhang, C. J.; Baxter, R. J.; Hu, P.; Alavi, A.; Lee, M. H. A Density Functional Theory Study of Carbon Monoxide Oxidation on the $Cu_3Pt(111)$ Alloy Surface: Comparison with the Reactions on Pt(111) and Cu(111). *J. Chem. Phys.* **2001**, *115*, 5272−5277.
(42) Rao, C. V.; Cabrera, C. R.; Ishikawa, Y. Graphene-Supported Pt-Au Alloy Nanoparticles: A Highly Efficient Anode for Direct Formic Acid Fuel Cells. *J. Phys. Chem. C* **2011**, *115*, 21963−21970.
(43) Xu, J. B.; Zhao, T. S.; Liang, Z. X. Carbon Supported Platinum-Gold Alloy Catalyst for Direct Formic Acid Fuel Cells. *J. Power Sources* **2008**, *185*, 857−861.
(44) Obradović, M. D.; Rogan, J. R.; Babić, B. M.; Tripković, A. V.; Gautam, A. R.S.; Radmilović, V. R.; Gojković, S. L. Formic Acid Oxidation on Pt-Au Nanoparticles: Relation between the Catalyst Activity and the Poisoning Rate. *J. Power Sources* **2012**, *197*, 72−79.
(45) Zhang, K.; Ren, F. F.; Wang, H. W.; Wang, C. Q.; Zhu, M. S.; Du, Y. K. Facile Synthesis of Gold-Modified Platinum Catalysts with High Performance for Formic Acid Electro-Oxidation. *ChemPlusChem* **2015**, *80*, 529−535.
(46) Park, I. S.; Lee, K. S.; Choi, J. H.; Park, H. Y.; Sung, Y. E. Surface Structure of Pt-Modified Au Nanoparticles and Electrocatalytic Activity in Formic Acid Electro-Oxidation. *J. Phys. Chem. C* **2007**, *111*, 19126−19133.
(47) Cuesta, A.; Cabello, G.; Osawa, M.; Gutiérrez, C. Mechanism of the Electrocatalytic Oxidation of Formic Acid on Metals. *ACS Catal.* **2012**, *2*, 728−738.
(48) Cuesta, A.; Cabello, G.; Hartl, F. W.; Escudero-Escribano, M.; Vaz-Domínguez, C.; Kibler, L. A.; Osawa, M.; Gutiérrez, C. Electrooxidation of Formic Acid on Gold: An ATR-SEIRAS Study of the Role of Adsorbed Formate. *Catal. Today* **2013**, *202*, 79−86.
(49) Zhang, J.; Sasaki, K.; Sutter, E.; Adzic, R. R. Stabilization of Platinum Oxygen-Reduction Electrocatalysts Using Gold Clusters. *Science* **2007**, *315*, 220−222.
(50) Yin, M.; Huang, Y. J.; Lv, Q.; Liang, L.; Liao, J. H.; Liu, C. P.; Xing, W. Improved Direct Electrooxidation of Formic Acid by Increasing Au Fraction on the Surface of PtAu Alloy Catalyst with Heat Treatment. *Electrochim. Acta* **2011**, *58*, 6−11.
(51) Obradović, M. D.; Tripković, A. V.; Gojković, S. L. The Origin of High Activity of Pt-Au Surfaces in the Formic Acid Oxidation. *Electrochim. Acta* **2009**, *55*, 204−209.
(52) Huang, J. S.; Hou, H. Q.; You, T. Y. Highly Efficient Electrocatalytic Oxidation of Formic Acid by Electrospun Carbon Nanofiber-Supported Pt_xAu_{100-x} Bimetallic Electrocatalyst. *Electrochem. Commun.* **2009**, *11*, 1281−1284.
(53) Singh, S.; Li, S.; Carrasquillo-Flores, R.; Alba-Rubio, A. C.; Dumesic, J. A.; Mavrikakis, M. Formic Acid Decomposition on Au Catalysts: DFT, Microkinetic Modeling, and Reaction Kinetics Experiments. *AIChE J.* **2014**, *60*, 1303−1319.
(54) Zhong, W. H.; Liu, Y. X.; Zhang, D. Theoretical Study of Methanol Oxidation on the PtAu(111) Bimetallic Surface: CO Pathway vs Non-CO Pathway. *J. Phys. Chem. C* **2012**, *116*, 2994−3000.
(55) Delley, B. An All-Electron Numerical Method for Solving the Local Density Functional for Polyatomic Molecules. *J. Chem. Phys.* **1990**, *92*, 508−517.
(56) Delley, B. From Molecules to Solids with the $Dmol^3$ Approach. *J. Chem. Phys.* **2000**, *113*, 7756−7764.
(57) Perdew, J. P.; Chevary, J. A.; Vosko, S. H.; Jackson, K. A.; Pederson, M. R.; Singh, D. J.; Fiolhais, C. Atoms, Molecules, Solids, and Surfaces: Applications of the Generalized Gradient Approximation for Exchange and Correlation. *Phys. Rev. B: Condens. Matter Mater. Phys.* **1992**, *46*, 6671−6687.
(58) Perdew, J. P.; Burke, K.; Ernzerhof, M. Generalized Gradient Approximation Made Simple. *Phys. Rev. Lett.* **1996**, *77*, 3865−3868.
(59) Gao, W.; Keith, J. A.; Anton, J.; Jacob, T. Theoretical Elucidation of the Competitive Electro-Oxidation Mechanisms of Formic Acid on Pt(111). *J. Am. Chem. Soc.* **2010**, *132*, 18377−18385.
(60) Luo, Q. Q.; Feng, G.; Beller, M.; Jiao, H. J. Formic Acid Dehydrogenation on Ni(111) and Comparison with Pd(111) and Pt(111). *J. Phys. Chem. C* **2012**, *116*, 4149−4156.
(61) Zhong, W. H.; Qi, Y. Y.; Deng, M. S. The Ensemble Effect of Formic Acid Oxidation on Platinum-Gold Electrode Studied by First-Principles Calculations. *J. Power Sources* **2015**, *278*, 203−212.
(62) Luo, Q. Q.; Wang, T.; Beller, M.; Jiao, H. J. Hydrogen Generation from Formic Acid Decomposition on Ni(211), Pd(211) and Pt(211). *J. Mol. Catal. A: Chem.* **2013**, *379*, 169−177.
(63) Bergner, A.; Dolg, M.; Küchle, W.; Stoll, H.; Preuß, H. Ab Initio Energy-Adjusted Pseudopotentials for Elements of Groups 13−17. *Mol. Phys.* **1993**, *80*, 1431−1441.
(64) Govind, N. J.; Petersen, M.; Fitzgerald, G.; King-Smith, D.; Andzelm, J. A Generalized Synchronous Transit Method for Transition State Location. *Comput. Mater. Sci.* **2003**, *28*, 250−258.
(65) Li, J.; Zheng, H. Y.; Zhang, X. C.; Li, Z. First-principles investigation on Cu/ZnO catalyst precursor: Energetic, structural and electronic properties of Zn-doped $Cu_2(OH)_2CO_3$. *Comput. Mater. Sci.* **2015**, *96*, 1−9.
(66) Kim, H. K.; Yang, J. W.; Jo, S. B.; Kang, B.; Lee, S. K.; Bong, H.; Lee, G.; Kim, K. S.; Cho, K. Substrate-Induced Solvent Intercalation for Stable Graphene Doping. *ACS Nano* **2013**, *7*, 1155−1162.
(67) Valentin, C. D.; Pacchioni, G.; Selloni, A. Theory of Carbon Doping of Titanium Dioxide. *Chem. Mater.* **2005**, *17*, 6656−6665.
(68) Yu, Y. L.; Wang, X.; Lim, K. H. A DFT Study on the Adsorption of Formic Acid and Its Oxidized Intermediates on (100) Facets of Pt, Au, Monolayer and Decorated Pt@Au Surfaces. *Catal. Lett.* **2011**, *141*, 1872−1882.
(69) Zhang, R. G.; Liu, H. Y.; Wang, B. J.; Ling, L. X. Insights into the Preference of CO_2 Formation from HCOOH Decomposition on Pd Surface: A Theoretical Study. *J. Phys. Chem. C* **2012**, *116*, 22266−22280.
(70) Wang, Y. Y.; Qi, Y. Y.; Zhang, D. J.; Liu, C. B. New Insight into the Decomposition Mechanism of Formic Acid on Pd(111): Competing Formation of CO_2 and CO. *J. Phys. Chem. C* **2014**, *118*, 2067−2076.
(71) Jeroro, E.; Vohs, J. M. Reaction of Formic Acid on Zn-Modified Pd(111). *Catal. Lett.* **2009**, *130*, 271−277.
(72) Grabow, L. C.; Gokhale, A. A.; Evans, S. T.; Dumesic, J. A.; Mavrikakis, M. Mechanism of the Water Gas Shift Reaction on Pt: First Principles, Experiments, and Microkinetic Modeling. *J. Phys. Chem. C* **2008**, *112*, 4608−4617.
(73) Hu, C. Q.; Ting, S. W.; Chan, K. Y.; Huang, W. Reaction Pathways Derived from DFT for Understanding Catalytic Decomposition of Formic Acid into Hydrogen on Noble Metals. *Int. J. Hydrogen Energy* **2012**, *37*, 15956−15965.
(74) Greeley, J.; Nørskov, J. K.; Mavrikakis, M. Electronic Structure and Catalysis on Metal Surfaces. *Annu. Rev. Phys. Chem.* **2002**, *53*, 319−348.
(75) Hammer, B.; Nørskov, J. K. Theoretical Surface Science and Catalysis−Calculations and Concepts. *Adv. Catal.* **2000**, *45*, 71−129.
(76) Berg, C.; Venvik, H. J.; Strisland, F.; Ramstad, A.; Borg, A. Nucleation and Growth of Au Overlayers on Pt(100)-Hex-R0.7° Studied by STM and Photoelectron Spectroscopy. *Surf. Sci.* **1998**, *409*, 1−15.
(77) Qi, Y. Y.; Li, J. J.; Zhang, D. J.; Liu, C. B. Reexamination of Formic Acid Decomposition on the Pt(111) Surface Both in the

DOI: 10.1021/acs.jpcc.5b10831
J. Phys. Chem. C 2016, 120, 2234−2246

Absence and in the Presence of Water, from Periodic DFT Calculations. *Catal. Sci. Technol.* **2015**, *5*, 3322−3332.
(78) Cuesta, A.; Escudero, M.; Lanova, B.; Baltruschat, H. Cyclic Voltammetry, FTIRS, and DEMS Study of the Electrooxidation of Carbon Monoxide, Formic Acid, and Methanol on Cyanide-Modified Pt(111) Electrodes. *Langmuir* **2009**, *25*, 6500−6507.
(79) Yuan, D. W.; Gong, X. G.; Wu, R. Q. Decomposition Pathways of Methanol on the PtAu(111) Bimetallic Surface: A First-Principles Study. *J. Chem. Phys.* **2008**, *128*, 064706−1−5.
(80) Kitchin, J. R.; Nørskov, J. K.; Barteau, M. A.; Chen, J. G. Modification of the Surface Electronic and Chemical Properties of Pt(111) by Subsurface 3d Transition Metals. *J. Chem. Phys.* **2004**, *120*, 10240−10246.
(81) Li, M.; Liu, P.; Adzic, R. R. Platinum Monolayer Electrocatalysts for Anodic Oxidation of Alcohols. *J. Phys. Chem. Lett.* **2012**, *3*, 3480−3485.
(82) Kitchin, J. R.; Nørskov, J. K.; Barteau, M. A.; Chen, J. G. Role of Strain and Ligand Effects in the Modification of the Electronic and Chemical Properties of Bimetallic Surfaces. *Phys. Rev. Lett.* **2004**, *93*, 156801-1−4.
(83) Ahn, S. H.; Liu, Y.; Moffat, T. P. Ultrathin Platinum Films for Methanol and Formic Acid Oxidation: Activity as a Function of Film Thickness and Coverage. *ACS Catal.* **2015**, *5*, 2124−2136.
(84) Kristian, N.; Yu, Y. L.; Gunawan, P.; Xu, R.; Deng, W. Q.; Liu, X. W.; Wang, X. Controlled Synthesis of Pt-Decorated Au Nanostructure and its Promoted Activity Toward Formic Acid Electro-Oxidation. *Electrochim. Acta* **2009**, *54*, 4916−4924.
(85) Kristian, N.; Wang, X. Pt_{shell}−Au_{core}/C Electrocatalyst with a Controlled Shell Thickness and Improved Pt Utilization for Fuel Cell Reactions. *Electrochem. Commun.* **2008**, *10*, 12−15.
(86) Kim, J.; Jung, C.; Rhee, C. K.; Lim, T. Electrocatalytic Oxidation of Formic Acid and Methanol on Pt Deposits on Au(111). *Langmuir* **2007**, *23*, 10831−10836.
(87) Banerjee, I.; Kumaran, V.; Santhanam, V. Synthesis and Characterization of Au@Pt Nanoparticles with Ultrathin Platinum Overlayers. *J. Phys. Chem. C* **2015**, *119*, 5982−5987.

DOI: 10.1021/acs.jpcc.5b10831
J. Phys. Chem. C 2016, 120, 2234−2246